

# TIM: Tree Imaging Machine for high resolution rapid digital images of tree cores and cookies

Adam Fong,<sup>1</sup> Chloe Curry,<sup>1</sup> Yue Zhang<sup>1,2</sup> and E.M. Wolkovich<sup>1</sup>

January 28, 2026

<sup>1</sup>Forest and Conservation Sciences, University of British Columbia, Vancouver, BC, Canada

<sup>2</sup>Department of Computer Science and Engineering, University of California San Diego, La Jolla, CA, USA

## Abstract

1. Studies of tree rings from climatology to ecology have become increasingly important with anthropogenic climate change, with a need for more research across more locations and species. Meeting the increasing demand requires methods to image wood samples rapidly and efficiently, while also producing high quality high resolution images.

2. Here we present the Tree Imaging Machine (TIM)—a do-it-yourself fully open scanning tool to digitize tree cookies and cores. TIM takes partially overlapping microscopic images of samples and stitches the individual images together to form a mosaic, which can be zoomed in to visualize features on the scale of 0.01 mm. We provide all instructions for the open-source hardware, using readily available parts, alongside the related software.

3. With scans of up to 21 140 DPI (0.83 pixels per micron), TIM produces one of the highest resolution images among similar tools for less than \$3 000 USD. Operators can prepare multiple samples to be scanned in a batch, letting the machine work until the queue is finished. Given this batch approach and automatic stitching, TIM provides a major speed advance for high-resolution image capture of tree rings, and can rapidly digitize cores of over 50 cm and complete cookies.

4. TIM provides a new method to gather high quality tree ring images at larger sizes and dimensions, integrating higher scanning resolution, tree cookie sampling, and batch digitization in a single low-cost package. Designed as completely open-source, we hope TIM will facilitate the widespread sampling of tree rings across diverse ecosystems and reduce barriers for researchers with smaller budgets.

## 1 Introduction

Incremental growth rings from trees have provided valuable insights into the abiotic and biotic environment across multiple fields—from climatology to forestry and ecology. Dated tree rings from dendrochronology have been critical to reconstructing past climates of regional and local environments, providing the most accurate, precise, and

reliable dating among alternatives (Mann *et al.*, 1999), and thus informing our understanding of climate change today (Fritts, 1971; Williams *et al.*, 2010; Guibal & Guiot, 2021; Sheppard, 2010; Williams *et al.*, 2020). Tree rings are also increasingly used in ecology to understand how plant competition affects tree growth in addition to climate (Buechling *et al.*, 2017) and have implications in forestry to managing stand dynamics (Canham *et al.*, 2004). These fields have leveraged two basic types of tree sampling techniques to capture the variation of tree rings: cores, which are cylindrical samples collected using an incremental borer, and ‘cookies,’ which are entire cross sections (and thus allow measuring as many radii from the sample as desired, Speer, 2010). As understanding tree growth and managing forest becomes more critical to mitigating climate change, scaling up the collection and processing of tree ring samples has become increasingly important.

The first computer-based method to measure tree ring widths used a microcomputer, a stage micrometer, and a push button, and is still used today. To acquire data, a trained technician shifts a core underneath a microscope objective and pushes a button connected to a microcomputer to record a ring’s location (Robinson & Evans, 1980). This method has high precision, but depends heavily on specific technicians and maintains no image record, preventing later measurement reproducibility and uncertainty quantification (Levanič, 2007).

Image analysis of tree rings was later implemented to reduce both errors in sampling and sampling bias across individual technicians, with major methods developed in the 1980s and 1990s to digitize tree ring samples using optical scanning (McMillin, 1982; Guay *et al.*, 1992). Optical scanners are still readily available for purchase, using a top of the line scanner (e.g., Epson Perfection V850 Pro) produces a maximum resolutions of 6 400 dpi and scan area of up to 21.6 cm x 29.7 cm. More recent techniques have aimed to achieve higher resolutions and/or larger samples through a different digitization approach—using an image-capturing system. These systems rely on a microscope camera to take images, motors to move the sample or camera, a computer to manage the capturing, and a second, more powerful, computer to stitch images into a larger composite image. Decreasing the field of view of each captured image increases the resolution of the final stitched image without restricting the size of the sample (Muhlich *et al.*, 2022). Stitching multiple images into one mosaic is a common technique used in other fields such as mineralogy and cellular biology (Ro & Kim, 2021), which was first implemented for tree rings through the Advanced Tree-Ring Image Capturing System (ATRICS) (Levanič, 2007).

Since ATRICS was introduced in 2007, image capture and stitching of tree rings have become more common. Today CaptuRING offers a more modern do-it-yourself alternative to ATRICS, creating scans up to 5 339 dpi using a DSLR camera and motorized stage (García-Hidalgo *et al.*, 2022). Another alternative, Gigapixel, achieves an impressive 19 812 dpi with the same DSLR image capture and composite stitch method (Griffin *et al.*, 2021). While CaptuRING and Gigapixel both use DSLR cameras and motorized movement, they differ on two fronts. First, Gigapixel’s camera is traversed across a stationary sample while CaptuRING moves a core sample underneath a stationary camera. With a mobile camera, multiple samples can be recorded sequentially without needing to remove a sample from a stage upon image completion—significantly reducing the active setup time for an operator. Second, Gigapixel automatically stitches individual images together once imaging is complete. This removes the need to transfer images to a more powerful computer for stitching as is necessary with CaptuRING. Additionally, both of these systems are designed to capture images along a singular axis as the entire width of a core fits within a single image’s field of view. This assumption fundamentally restricts

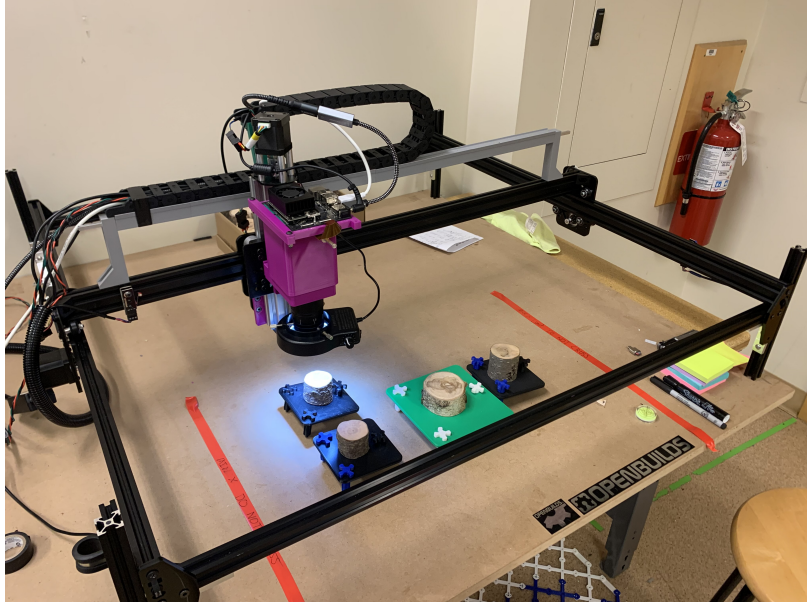


Figure 1: Complete assembly of TIM, shown with a few smaller cookies ready to be scanned. All of the 3D printed parts are available for download on the NIH 3D printing repository and the software is open source, with instructions to recreate this tool available on GitHub.

the digitization only to cores, as cookies have a two dimensional scanning surface.

To address some of the current limitations, while building upon the open-source and open-hardware philosophies of CaptuRING, we designed the Tree Imaging Machine (TIM). We added support to digitize both cookies and cores, increased the maximum sample length, perform image stitching directly without the need for manual file transfer, and capture batches of samples sequentially—all while minimizing cost. Our design requires the use of 3D printed components and common hand tools such as hex keys and wrenches. No specialized equipment or power tools are required beyond this. Excluding 3D printed parts, the total cost of the machine is approximately \$2 200 USD (compared to the \$70 000 USD of the Gigapixel, Griffin *et al.*, 2021). We chose to use a Raspberry Pi HQ camera with a microscope lens to save on purchasing a professional camera with a macro lens. Professional camera setups are comparable in price to the entire cost of TIM. These savings combined with not needing to purchase a professional stitching software license (such as PTGui from New House Internet Services BV, Rotterdam, NL, which is the suggested software to use with CaptuRING) makes TIM a more economical option than most products current available. Additionally the design is open-source and open-hardware allowing for contributors to add new sensors or alter the control methods.

## 2 Methods

### 2.1 TIM System Overview

TIM can be thought of as a combination of multiple subsystems: a gantry machine, camera, and computer (Figure 1). For the gantry machine, cartesian movement in the  $X$ ,  $Y$  and  $Z$  directions is a result of two machine kits and a motor controller from OpenBuilds—the ACRO 1010, the NEMA 17 lead screw linear actuator, and the X32

Motor Controller running Grbl firmware. The machine kit includes extruded aluminum rails, carriages to slide along the rails, stepper motors to control the  $X$  and  $Y$  movement, and all the hardware to assemble the machine. To fit on the end-effector plates of the ACRO system, we made an adapter to connect the linear actuator to the  $X$  and  $Y$  axis, thus creating motion in the  $Z$  axis. The size of the work plane is ultimately up to the size of the ACRO kit that is purchased—allowing for more flexibility. Building on top of kits allowed for quick assembly with sound instructions and saved development time. For the camera, we chose a 12MP Raspberry Pi HQ Camera equipped with a SEEED studio microscope lens with adjustable focal length resulting in up to 150x zoom. The focal length was adjusted to make the field of view approximately 3 mm by 5 mm height and width. The camera was connected to the gantry machine using custom, 3D printed, adapters. For the computer, we implemented all of the software control, image stitching, and graphical user interface (GUI) to run on an NVIDIA Jetson Orin Nano 8GB (Jetson edge computer), which also connects to the camera via a MIPI cable.

By choosing this combination, we were able to reduce the weight and cost of the camera significantly. This minimized the design challenges of stabilizing the movement of a heavier DSLR and allowed us to invest more in a powerful computer that can handle intensive image processing. The Jetson is an edge computer which drives a monitor for a GUI, sends commands to the motor controller to move the machine, runs image processing calculations for machine control, and performs calculations to stitch individual images into one mosaic.

## 2.2 Preparing Cookies and Cores

TIM can scan both tree cookies and tree cores but they need to be well prepared before scanning. Samples that are not well sanded may not have enough detail when stitching images together into the complete mosaic. The general guidelines used for preparing cookies and cores applies—requiring samples to be sanded with incrementally increasing sand paper grit. Samples must be uniformly sanded and have planar surface for scanning (Speer, 2010). We sanded samples using a 4 inch belt sander with lower grits between 120 and 240 for the bulk of the material removal. An orbital sander was used to sand the finer grits between 240 and 400. We then used a microscope to visually inspect the quality of the sanding. Samples were considered to be sufficiently prepared when vessels were easily recognizable.

TIM requires additional sanding considerations for each sample type. For cookies, it is important to have the top and bottom surfaces nearly parallel. Small differences in plane angle can be corrected using the 3D printed leveling table we designed (Figure 2a).

For cores, care should be taken to maximize the scanning surface. This means removing material to be coincident to the center of the cross section of the core. Similarly to cookies, the scanning surface should be as close to parallel to the XY-plane as possible, but generally does not need to be leveled using the leveling tables.

## 2.3 Scanning Samples

TIM can scan cores, cookies, and sections of cookies. Each one of these scans requires a slightly different process, which we describe in separate subsections. A few principles are common regardless of what is being scanned, and we describe these first.

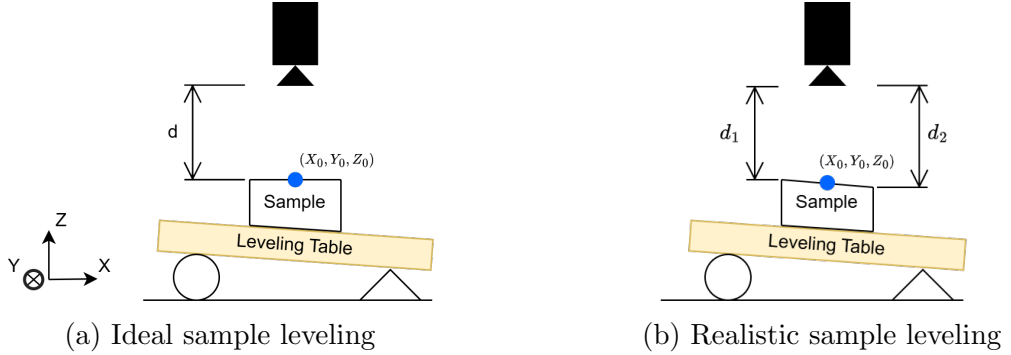


Figure 2: Side view of the camera (top, in black) and sample on top of a leveling table. The ideal sample leveling shows a uniform distance,  $d$ , at all  $XY$  coordinates on the sample. This is impossible to achieve in reality, the true sample leveling has a non-uniform distance at unique  $XY$ .

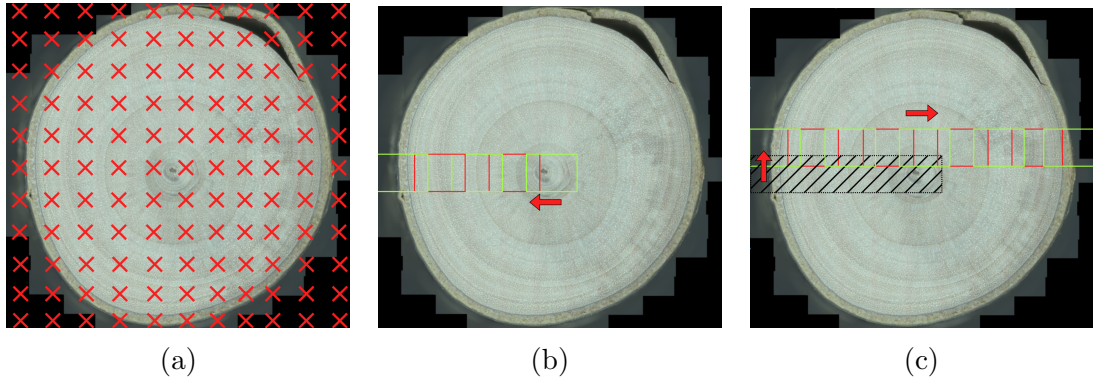


Figure 3: An example imaging process of a cookie sample in two dimensions. Here, the height and width of the capture region enclose the entire surface area of the cookie. TIM begins by generating a grid of target coordinates to systematically capture a grid of continuous and partially overlapping images (a). TIM takes its first image at the center coordinate of the sample, then the rectangular field of view from the camera moves to adjacent target coordinates until it reaches the left boundary—capturing an image for each target coordinate (b). After completing the row, TIM moves to a new row and continues capturing adjacent images (c).

### 2.3.1 Regions of Overlap for Stitching

The individual images from TIM have a field of view of approximately 3 mm x 5 mm. Because cores and cookies can be many orders of magnitude larger than one of these images, the final scan of these samples will be the combination of many images stitched together. Stitching two images together requires both images to share a region of overlap in which the subject of the image is the same (Mohammadi *et al.*, 2024). Unique features inside this region of overlap act as a map to connect the two images. By default TIM is set to have a 33% overlap with its neighbor but this can be adjusted easily while adding a sample in the GUI.

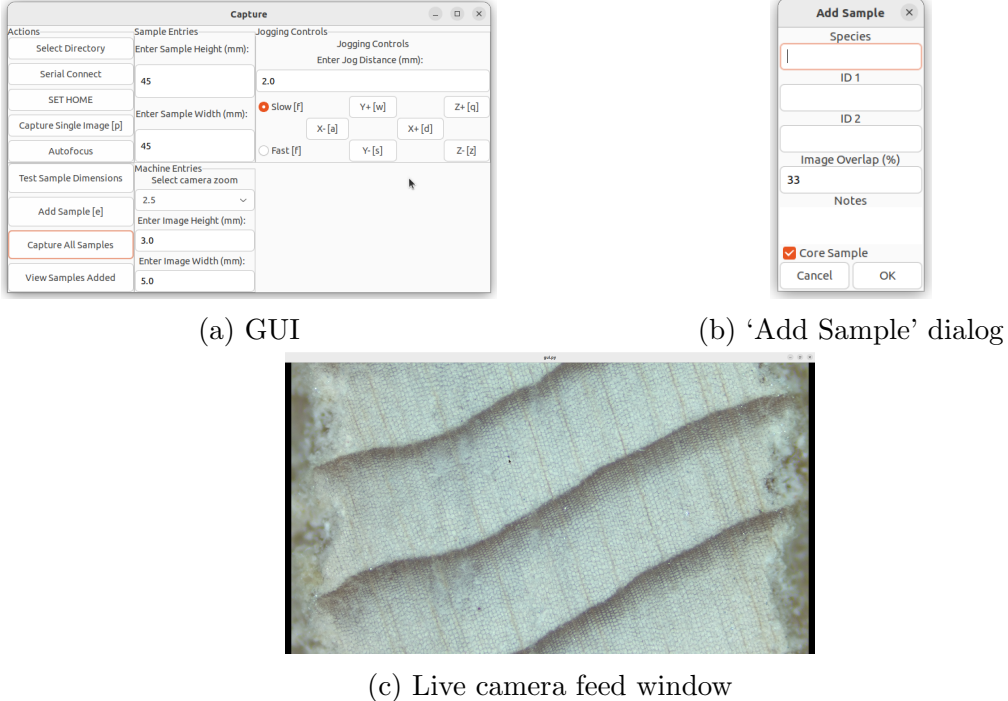


Figure 4: TIM is controlled using a GUI, popup windows, and a live camera feed.

### 2.3.2 Golden Section Search Autofocusing

Most microscope lenses are a fixed focal length, requiring the subject to be moved in relation to the lens for focusing. Additionally, inexpensive microscope lenses often have a very small depth of field. Variations of height across the length of a sanded sample result in images losing focus during a scan (Figure 2b). An autofocus algorithm was implemented using a Golden Section Search method as described by (Gu *et al.*, 2015) to capture in-focus images. In short, the camera’s position is moved in the  $Z$  axis and stops when it maximizes the sharpness metric of the image. We found the variance of Laplacian sharpness metric to be easy to implement in Python and robust across samples (Pech-Pacheco *et al.*, 2000).

### 2.3.3 Core Scanning Procedure

Scanning a core starts with aligning the length of the sample to the  $Y$ -axis of the machine at any  $X$  position. We 3D printed a tray to hold multiple cores next to each other to make the alignment process faster. From there, the operator needs to navigate the camera to an in-focus position anywhere along the core and enter basic metadata such as sample ID. Multiple cores can be put next to each other and added to a queue to be sequentially scanned for operational convenience.

A button on the GUI will start the procedure to scan all of the samples that were added to the queue. The machine first moves to the position that was recorded when the operator added the sample. It then moves up the length of the core in the positive direction of the  $Y$ -axis, capturing overlapping images until the top edge of the core is captured. TIM then returns back to the starting location, repeating the imaging procedure in the negative direction of the  $Y$ -axis until encountering the bottom edge of the core.

The top and bottom edges of the core are detected by comparing the sharpness metric to a configurable threshold. When the camera moves past either edge of a core, there is no subject in the focused plane of the lens. These images are very blurry and the sharpness metric is at least an order of magnitude less than the images that are focused on the core. If the Golden Section Search algorithm only finds images with a sharpness metric lower than this threshold, it is safe to assume the sample is no longer in the frame. The same threshold was used across all cores across 5 species that we have scanned, but tuning may be required to prevent false positives. This technique reduces scanning setup time as the operator does not need to measure the length of each core when adding the sample into scanning queue.

Golden Section Search autofocusing is robust, but takes up to 10 seconds to get the most in-focus image in our implementation. When capturing tens or hundreds of images per sample, autofocusing time becomes significant. In the interest of minimizing scanning time per sample, we chose to only autofocus when necessary. Autofocusing occurs on the very first image to get a baseline sharpness metric. The machine then moves to capture the neighboring image. If the new image has at least a sharpness metric of 95% of its previously imaged neighbor, we choose not to run the autofocusing loop. If the prepared surface of the core is perfectly planar to the table that TIM is installed on, it is possible to only autofocus once for tens of images. With the samples we prepared, there usually needed to be an autofocusing procedure for every 5-10 images.

#### 2.3.4 Accounting for Translation Error Between Core Samples

Movement accuracy issues arise when more than one core is added to the digitization queue. While the ACRO has a theoretical 4.5 micron translational accuracy, the machine still sometimes over- or under-shoots the true location when moving to a stored location of the core—resulting in the core not being centered in the frame. We thus implemented a centering procedure that realigns the center of the core to the center of the image frame when the machine moves to a new sample.

The goal with the recentering procedure is to prevent the scan from including significant portions of blurry background. This process works by creating a region of interest in a horizontal strip through the center of the image. The strip is further segmented into multiple subsections aligned in a row. In each of the subsections, the sharpness metric is calculated. Subsections with very low sharpness are likely to be background. If background is detected in the left most or right most subsections, corrective movements in the  $X$  direction are made to recenter the core.

#### 2.3.5 Cookie Scanning Procedures

Cookies can be both partially and completely scanned. Scanning entire cookies is possible and requires the operator to define a minimum bounding box using the Sample Height and Sample Width text boxes in the GUI. Additionally, the operator must navigate the camera to the center of the cookie before adding the sample to the queue. A button called “Test Cookie Boundaries” was made to trace the bounding box of the cookie for the operator to verify that the sample is truly within the bounds. These height and width bounds are used to calculate where the machine needs to move to achieve a set of partially overlapping images in both directions.

The file sizes of entire cookie scans can quickly become too large to analyze with commonly available software. A full resolution scan (21 140 DPI) of a 10 cm x 10 cm

cookie is multiple gigabytes in a lossless file format. TIM can adjust the resolution of the final scan to be any percentage of the maximum DPI if needed. Whole cookie scans are interesting for archiving but will need special considerations for most samples at high resolution.

Portions of cookies can be scanned by treating them as if they were a core. This can be done by aligning the pith of the cookie's major or minor axis to the  $Y$  axis and using the core scanning procedure. Any radius of the cookie can be scanned this way.

### 2.3.6 Image Stitching

Image stitching is a well explored field, ranging from panoramic images taken on smart phones to highly tuned microscopy slide stitching. Stitching one image to another requires both to share a region of overlap. When capturing a sample using TIM, the operator has the ability to choose a percentage amount of overlap between images. Most samples are digitized with a percentage overlap between 33% and 50%.

After testing numerous image stitching softwares, we found the Python package Stitch2D most capable of stitching our images successfully (Mansur, 2022). This package wraps OpenCV functions for finding distinctive image features using the scale-invariant feature transform (SIFT) method and matches these features within the overlapping region of adjacent images (Lowe, 2004). The default implementation of the package produces high quality stitches but is memory inefficient. We implemented a few key memory-conscious changes such as loading only one image into RAM at a time and writing the final image to a memory-mapped NumPy file before converting to a TIFF file. These changes allowed for the package to run without being limited by RAM on a Jetson edge computer without a problem.

Some tree ring analyses may not need the maximum scanning resolution produced by TIM. At maximum resolution, TIM's scans quickly produce large file sizes and can be costly to store at scale. To address this, a parameter in the machine configuration file allows the operator to choose a downsizing ratio to apply to images before they are stitched, decreasing the file size of the scans. With the same images, multiple final stitched resolutions can be made.

## 2.4 Scanning Hard-to-Stitch Samples

We found some samples were impossible to scan without additional preparation. The most common scenario leading to an incomplete scan was due to regions of the core having few distinguishable SIFT features. Samples often begin to lack features when focusing on lightly-colored sapwood. SIFT features may also lack where there are sanding blemishes or other imperfections on the scanning surface. In such cases, we developed a particle smearing method which add features to the sample, aiding the stitching process.

### 2.4.1 Particle Smearing

The ideal method for adding features to the sample is to smear small particles with contrasting color compared to the surface of the sample. Our powder of choice was 600 mesh silicon carbide powder as it is inexpensive, available at pottery supply stores, has reliable grain sizes smaller than the finest sand paper we used, and provides good color contrast with most wood. Additionally, silicon carbide is very hard so it will not be broken into smaller grains when smearing into the surface of the sample.



(a) Without powder smearing



(b) With powder smearing

Figure 5: A hard-to-scan sample with and without silicon carbide smeared on the surface of the core.

No extra tools are needed for this method—a fingertip dipped in the powder is sufficient. The powder should be smeared across the sample’s sanded surface, smoothing any clumps of powder in the process. When applied correctly, trace amounts of silicon carbide will be embedded in the surface roughness of the sample which can not be seen without microscope magnification. Images of a core before and after powder smearing can be seen in Figure 5. Most of the silicon carbide can be removed after scanning is complete by blowing compressed air on the sample.

### 3 Results & Discussion

TIM is capable of producing extremely high resolution scans. We calculated the maximum dots per inch (DPI) at 21 500 of individual images captured from the system using a microscopy slide scale (with 0.01 mm graduations, Figure S1), and developed a Python tool to replicate this for varied lens focal lengths. When downscaling the final stitch, DPI scales linearly with the downscale percentage defined in the machine parameters.

Digitizing samples takes significantly longer for cookies than it does for cores (Figure 6). This is due to the surface area of cookies requiring more images, as it has a square relationship to sample radius. For large cookies, the operator can choose to selectively scan a radius of the cookie instead of the whole surface. A single radius contains a portion of each ring. Scanning complete cookies at maximum DPI is unrealistic as file size limits are quickly encountered with small diameter cookies.

To fit into the maximum 2.5 GB limits of a TIFF file, the maximum diameter of a cookie scanned at 30% of maximum resolution is limited to approximately 130 mm. This maximum cookie diameter is significantly smaller than the maximum core sample length. At maximum resolution, the file size limit constrains core samples to approximately 1 500 mm in length (though a larger ACRO frame than shown here would be needed to support this sample length). Samples larger than this limit can still be scanned, but TIM saves them as an uncompressed binary NumPy memory-mapped array file. Currently, NumPy files are not supported by standard image viewers like ImageJ and require custom tools to work with.

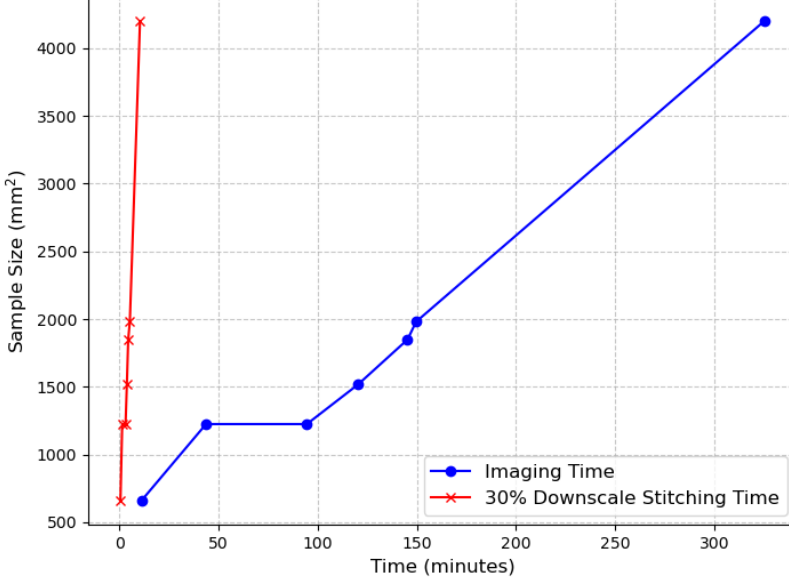


Figure 6: Time to digitize a sample is dependent on the sample’s surface area and the desired final resolution. Cores benefit from linear surface area to sample length. The range of samples included span from a 3 mm x 220 mm core to a 75 mm x 56 mm cookie. The theoretical maximum sample dimensions are limited by the working plane of the machine, approximately 500 mm x 500 mm in our configuration. True sampling times are drastically influenced by configurable machine parameters such as percentage image overlap.

### 3.1 Strengths and Opportunities

TIM’s design minimizes the barriers to build an affordable, efficient and high-resolution image capture system. TIM does not compromise scan quality and can scan both cookies and cores. We have measured tree ring widths using the digitized samples from TIM using CooRecorder as well as ImageJ (Schneider *et al.*, 2012), but the utility of these images could be extended through new open-data approaches. For example, while most tree ring repositories (e.g., the International Tree-Ring Data Bank or TreeSource’s Tree-Rings Database for Canadian sites Grissino-Mayer & Fritts, 1997; Girardin *et al.*, 2021) do not store the source images of samples currently, they provide rich metadata, which could be used to link to images stored on other more flexible repositories. Eventually extending these databases to include source images of cores and cookies (and annotating them in bulk), however, would be beneficial to field and potentially provide training data for deep learning models for vessel counting and tree ring boundary identification. Examples of such models exist and have the potential to significantly decrease the time invested in manually identifying tree anatomy (Resente *et al.*, 2021; Poláček *et al.*, 2023). With more robust identification models, TIM could be extended to run these models while scanning.

In its current state, TIM only provides scanned images and requires users to import them into other tools for additional visual analyses, such as measuring tree-ring widths or counting vessels. A useful addition to TIM would be to automatically detect tree-ring widths or other metrics while capturing images using computer vision models. We expect this may be possible as these methods improve in computational efficiency and accuracy. Currently, we found that tree-ring detection by a recent machine learning algorithm (R-CNN presented by Poláček *et al.*, 2023) for a scanned core (23294 x 897 pixels) took 15

minutes on a high-performance cluster (UBC ARC Sockeye) and 3.5 hours on a smaller server (RTX A6000 GPU server). Although the Jetson edge computer is not as powerful as these servers, running these models in parallel to the image capturing algorithms would further reduce manual data annotation of tree-rings, and thus could help scale-up data collection.

TIM relies on purchasing a CNC machine kit from OpenBuilds which is subject to availability. Fortunately, our software is compatible with any cartesian CNC machine controlled by the Grbl software, a common and open-source CNC motion controller software. Many alternative CNC kits are available but would require new adapters to be made to hold the lens, camera, and computer to the machine.

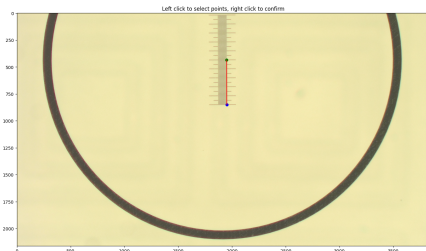
## 4 Conclusion

By taking advantage of a common three axis cartesian machine design, powerful edge computing, and a microscope camera we were able to design a cost effective and high resolution digitization tool for wood samples. Our design significantly increases the maximum sample length and maximum resolution compared to common alternatives in the field. In addition, TIM is intended to be readily replicated by labs without significant engineering capacity and equipment. We hope that such an open-source device will facilitate the widespread sampling of tree rings across diverse ecosystems and reduce barriers for researchers with smaller budgets.

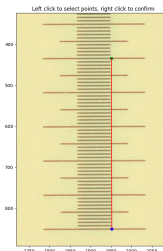
## 5 Acknowledgments

The authors thank Deirdre Loughnan, Hoai Huong Nguyen Phan, Frederik Baumgarten and Victor Van der Meersch for conversations, ideas and review to help bring this project to fruition. Additionally, we thank Xiaomao Wang and Christophe Rouleau-Desrochers for their help and patience in operating TIM during development.

## 6 Supplemental Information



(a) Scale Bar for DPI measurements



(b) Zoomed in Scale Bar

Figure S1: Example of a single DPI measurement using a 0.01 mm slide scale. We found the DPI measured at multiple locations in the field of view vertically and horizontally converged on the same value.

Terms	Definition
$X_0, Y_0, Z_0$	The initial cartesian coordinates of the camera when the sample is saved by the user.
$d_1$	The relative distance from the camera to one edge of a leveled sample (Figure 2).
$d_2$	The relative distance from the camera to the opposite edge of a leveled sample (Figure 2).

Table S1: Mathematical notation used in this paper.

## References

- Buechling, A., Martin, P.H. & Canham, C.D. (2017) Climate and competition effects on tree growth in Rocky Mountain forests. *Journal of Ecology* **105**, 1636–1647, eprint: <https://onlinelibrary.wiley.com/doi/pdf/10.1111/1365-2745.12782>.
- Canham, C.D., LePage, P.T. & Coates, K.D. (2004) A neighborhood analysis of canopy tree competition: effects of shading versus crowding. *Canadian Journal of Forest Research* **34**, 778–787, publisher: NRC Research Press.
- Fritts, H.C. (1971) Dendroclimatology and dendroecology. *Quaternary Research* **1**, 419–449.
- García-Hidalgo, M., García-Pedrero, , Colón, D., Sangüesa-Barreda, G., García-Cervigón, A.I., López-Molina, J., Hernández-Alonso, H., Rozas, V., Olano, J.M. & Alonso-Gómez, V. (2022) CaptuRING: A do-it-yourself tool for wood sample digitization. *Methods in Ecology and Evolution* **13**, 1185–1191, eprint: <https://onlinelibrary.wiley.com/doi/pdf/10.1111/2041-210X.13847>.
- Girardin, M.P., Guo, X.J., Metsaranta, J., Gervais, D., Campbell, E., Arsenault, A., Isaac-Renton, M., Harvey, J.E., Bhatti, J. & Hogg, E.H. (2021) A national tree-ring data repository for Canadian forests (CFS-TRenD): structure, synthesis, and applications. *Environmental Reviews* **29**, 225–241, publisher: NRC Research Press.
- Griffin, D., Porter, S.T., Trumper, M.L., Carlson, K.E., Crawford, D.J., Schwalen, D. & McFadden, C.H. (2021) Gigapixel Macro Photography of Tree Rings. *Tree-Ring Research* **77**, 86–94, publisher: Tree-Ring Society.
- Grissino-Mayer, H.D. & Fritts, H.C. (1997) The International Tree-Ring Data Bank: an enhanced global database serving the global scientific community. *The Holocene* **7**, 235–238, publisher: SAGE Publications Ltd.
- Gu, C.C., Wu, K.J., Hu, J., Hao, C. & Guan, X.P. (2015) Region sampling for robust and rapid autofocus in microscope. *Microscopy Research and Technique* **78**, 382–390, eprint: <https://analyticalsciencejournals.onlinelibrary.wiley.com/doi/pdf/10.1002/jemt.22484>.
- Guay, R., Gagnon, R. & Morin, H. (1992) A new automatic and interactive tree ring measurement system based on a line scan camera. *The Forestry Chronicle* **68**, 138–141.
- Guibal, F. & Guiot, J. (2021) Dendrochronology. *Paleoclimatology* (eds. G. Ramstein, A. Landais, N. Bouttes, P. Sepulchre & A. Govin), pp. 117–122, Springer International Publishing, Cham.
- Levanič, T. (2007) Atrics – A New System for Image Acquisition in Dendrochronology. *Tree-Ring Research* **63**, 117–122, publisher: Tree-Ring Society.
- Lowe, D.G. (2004) Distinctive Image Features from Scale-Invariant Keypoints. *International Journal of Computer Vision* **60**, 91–110.

- Mann, M.E., Bradley, R.S. & Hughes, M.K. (1999) Northern hemisphere temperatures during the past millennium: Inferences, uncertainties, and limitations. *Geophysical Research Letters* **26**, 759–762, \_eprint: <https://onlinelibrary.wiley.com/doi/pdf/10.1029/1999GL900070>.
- Mansur, A. (2022) Stitch2D.
- McMillin, C.W. (1982) Application of Automatic Image Analysis to WoodScience. *Wood Science* **14**, 97–105.
- Mohammadi, F.S., Mohammadi, S.E., Mojarrad Adi, P., Mirkarimi, S.M.A. & Shabani, H. (2024) A comparative analysis of pairwise image stitching techniques for microscopy images. *Scientific Reports* **14**, 9215, publisher: Nature Publishing Group.
- Muhlich, J.L., Chen, Y.A., Yapp, C., Russell, D., Santagata, S. & Sorger, P.K. (2022) Stitching and registering highly multiplexed whole-slide images of tissues and tumors using ASHLAR. *Bioinformatics (Oxford, England)* **38**, 4613–4621.
- Pech-Pacheco, J., Cristobal, G., Chamorro-Martinez, J. & Fernandez-Valdivia, J. (2000) Diatom autofocusing in brightfield microscopy: a comparative study. *Proceedings 15th International Conference on Pattern Recognition. ICPR-2000*, vol. 3, pp. 314–317 vol.3, iSSN: 1051-4651.
- Poláček, M., Arizpe, A., Hüther, P., Weidlich, L., Steindl, S. & Swarts, K. (2023) Automation of tree-ring detection and measurements using deep learning. *Methods in Ecology and Evolution* **14**, 2233–2242, \_eprint: <https://onlinelibrary.wiley.com/doi/pdf/10.1111/2041-210X.14183>.
- Resente, G., Gillert, A., Trouillier, M., Anadon-Rosell, A., Peters, R.L., von Arx, G., von Lukas, U. & Wilmking, M. (2021) Mask, Train, Repeat! Artificial Intelligence for Quantitative Wood Anatomy. *Frontiers in Plant Science* **12**, publisher: Frontiers.
- Ro, S.H. & Kim, S.H. (2021) An image stitching algorithm for the mineralogical analysis. *Minerals Engineering* **169**, 106968.
- Robinson, W.J. & Evans, R. (1980) A MICROCOMPUTER -BASED TREE -RING MEASURING SYSTEM. *Tree-Ring Bulletin* **40**.
- Schneider, C.A., Rasband, W.S. & Eliceiri, K.W. (2012) NIH Image to ImageJ: 25 years of image analysis. *Nature Methods* **9**, 671–675, publisher: Nature Publishing Group.
- Sheppard, P.R. (2010) Dendroclimatology: extracting climate from trees. *WIREs Climate Change* **1**, 343–352, \_eprint: <https://onlinelibrary.wiley.com/doi/pdf/10.1002/wcc.42>.
- Speer, J.H. (2010) *Fundamentals of Tree Ring Research*. University of Arizona Press.
- Williams, A.P., Cook, E.R., Smerdon, J.E., Cook, B.I., Abatzoglou, J.T., Bolles, K., Baek, S.H., Badger, A.M. & Livneh, B. (2020) Large contribution from anthropogenic warming to an emerging North American megadrought. *Science* **368**, 314–318, publisher: American Association for the Advancement of Science.
- Williams, A.P., Michaelsen, J., Leavitt, S.W. & Still, C.J. (2010) Using Tree Rings to Predict the Response of Tree Growth to Climate Change in the Continental United States during the Twenty-First Century Section: Earth Interactions.